Journal of Nuclear Materials 384 (2009) 19–24

Contents lists available at ScienceDirect

Journal of Nuclear Materials

journal homepage: www.elsevier.com/locate/jnucmat

Reaction kinetics of radiation-induced defects in vitreous silica under ion beam irradiation

Kimikazu Moritani, Jun Takemoto, Ikuji Takagi, M. Akiyoshi, Hirotake Moriyama *

Department of Nuclear Engineering, Graduate School of Engineering, Kyoto University, Yoshida, Sakyo-ku, Kyoto 606-8501, Japan

ARTICLE INFO

Article history:
Received 28 August 2007
Accepted 26 September 2008

PACS:
61.80.Jh
61.72.Cc

ABSTRACT

The production behavior of radiation-induced defects in vitreous silica was studied by an in-situ luminescence measurement technique under ion beam irradiation of He^+. The luminescence intensity of oxygen deficiency centers (ODCs) at 460 nm was observed to vary with irradiation time reflecting the accumulation behavior of the ODCs. The luminescence intensity increased after the start of irradiation and then decreased at room temperature, while it increased rapidly to a constant value at higher temperatures. Some differences were observed due to different OH contents in silica. The observations were analyzed by considering the production mechanisms and kinetics of the radiation-induced defects.

1. Introduction

Irradiation behavior of ceramic materials is one of the major topics, since some of these materials are to be used in the strong radiation field in proposed fusion reactors. However the dynamic production behavior of radiation-induced defects under irradiation has not been fully clarified in spite of the considerable progress in understanding many aspects of radiation-induced defects in the ceramic materials. It is thus important to know the production behavior of radiation-induced defects by such an in-situ measurement technique [1].

In our previous study [2], the production behavior of radiation-induced defects in vitreous silica was studied by an in-situ luminescence measurement technique under ion beam irradiation of H^+ and He^+. The temperature dependence of the steady-state luminescence intensity at 280 and 460 nm was measured, and analyzed by considering the production mechanisms and kinetics of the radiation-induced defects of oxygen deficiency centers (ODCs: ≡Si:Si≡). The analysis was based on some assumptions; the luminescence of ODCs was assumed to be observed only on their production and the first-order kinetics was assumed for the recombination reactions of ODCs. If the luminescence is only observed on producing the defect, and if there is no change in the efficiency or mechanism, the luminescence would be constant. However, this may not be the case for some emissions including the 460 nm emission of ODCs, the luminescence is more likely to be related to the total number of stable defects produced (or their counterpart, interstitials), as reported for alumina [3]. It is thus needed to check the validity of the earlier assumptions.

In the present study, similarly to the case of alumina [3], the irradiation time dependence of the luminescence intensity was measured of vitreous silica, and it was found that a considerable part of the luminescence comes from ODCs accumulated by irradiation. The observations were analyzed in order to improve our knowledge on the production mechanisms and kinetics of the radiation-induced defects.

2. Experimental

The specimens of vitreous silica were T-2030 (1 ppm OH) and T-4040 (800 ppm OH) obtained from Toshiba Ceramics Co Ltd., which were of 10 mm in diameter and about 0.5 mm in thickness, and were irradiated with He^+ ion beam, accelerated to 2 MeV with a Van de Graaff accelerator. The range and total number of displacements were estimated to be about 8 μm and 160 displacements/ion, respectively, by using the TRIM code (SRIM-98) with the displacement energies of 20 eV for Si and O. In some literatures, the dpa value, which varied along the Bragg curve, was evaluated by taking the values at the damage peak [4,5] and by taking the average ones in the region of a full-width at half maximum [6]. Similarly, by considering the displacement distribution $D(x)$ along the Bragg curve, a weighted average dpa value was obtained in the present study as $\mathrm{dpa} = [\int D(x)\mathrm{dpa}(x)\mathrm{d}x]/\int D(x)\mathrm{d}x$ where x denotes the depth. Then a conversion factor of 4.1×10^{20} ions m^{-2} dpa^{-1} for oxygen was obtained for 2 MeV He^+ ions. It should be noted that the weighted average dpa value was only for a representative input value to the rate equations and not for correlating the dpa value to optical property changes in the present study, and that

* Corresponding author. Tel.: +81 75 753 5824; fax: +81 75 753 5824.
E-mail address: moriyama@nucleng.kyoto-u.ac.jp (H. Moriyama).

0022-3115/$ - see front matter © 2008 Elsevier B.V. All rights reserved.
doi:10.1016/j.jnucmat.2008.09.025

Table 1
Experimental conditions.

Specimen	Irradiation condition		
	Projectile	Temperature[a] (K)	Beam current (10^{-3} A/m^2)
T-2030	2 MeV He^+	298–523	0.65–1.67
T-4040	2 MeV He^+	298–523	1.00–1.67

[a] Temperature of the thermocouple attached to the sample surface to monitor its temperature.

for the latter purpose the ion fluence and not the dpa was used. The size of the ion beam was about 4 mm in diameter and its current was monitored. The ion beam intensity was around 1.0×10^{-3} A m^{-2}, and the dose was up to 1.0×10^{20} ions m^{-2} (0.24 dpa). The specimens were irradiated at various temperatures from room temperature to 523 K. The luminescence from the target sample was measured with a photonic multichannel analyzer, Hamamatsu PMA-1165. The temperature of the sample holder was controlled with an electric heater and thermocouple while another thermocouple was attached to the sample surface to monitor its temperature at a distance close to beam area. In the room temperature irradiation, the temperature rise by beam heating was observed to be within a few degrees as estimated from the values of thermal diffusion coefficient, density and heat capacity of silica. After irradiation, some specimens were subjected to the optical absorption measurement using a UV-Vis spectrophotometer, Shimadzu MultiSpec-1500. The experimental conditions are summarized in Table 1.

3. Results and discussion

3.1. Irradiation time dependence

Fig. 1 shows typical luminescence spectra of T-2030 and T-4040 under 2 MeV He^+ irradiation at 298 K. Three bands are identified at 280 nm, 460 nm and 650 nm in each spectrum. According to the literature [7], the luminescence at 2.7 eV (460 nm) and 4.4 eV (280 nm) is attributed to the triplet (T_1 to S_0) and the singlet (S_1 to S_0) emissions of ODCs, respectively, and the luminescence at 1.9 eV (650 nm) to non-bridging oxygen hole centers (NBOHCs: ≡Si–O•Si≡). By comparing the luminescence intensities, it is noticed that the luminescence intensity at 460 nm is much larger than those at 280 nm and 650 nm.

Considering that the absorption bands are observed at 4.8, 5.02, 5.8, 7.15 and 7.6 eV in ion-irradiated silica [8], it is important to study the effect of the optical absorption on the luminescence spectra. Some specimens after irradiation were subjected to the absorption measurement in the present study. Fig. 2 shows the absorption spectra obtained for the specimens of T-2030 and T-4040 irradiated to 3.6×10^{19} ions m^{-2} at room temperature. Very similar spectra were obtained for both specimens irradiated to 1.3×10^{19} ions m^{-2}, indicating the saturated absorbance. No significant absorption was observed in the region from 350 to 800 nm, indicating negligible effect of the absorption on the luminescence intensities at 460 nm and 650 nm. In the UV region from 200 to 350 nm, on the other hand, the absorbance was observed suggesting the formation of the NBOHCs (4.8 eV) and ODCs (5.02 eV) [8]. It is thus needed to correct the observed luminescence intensity at 280 nm for a detailed analysis.

Fig. 3 shows the irradiation time dependences of the luminescence intensities at 460 nm and 650 nm for T-2030 and T-4040 at 298 K. Also, Fig. 4 shows the irradiation time dependences of the luminescence intensities at 460 nm for T-2030 at different temperatures up to 523 K. In these figures, the luminescence intensities at 460 nm and 650 nm are observed to change during irradiation although no apparent change is observed at 280 nm as mentioned below. In the case of T-2030 in Fig. 3(a), for example, it can be seen that the luminescence intensity increases after the start of irradiation and then decreases. By annealing the irradiated specimens above 1073 K for some 10 min, such irradiation histories have been observed repeatedly. This fact suggests that a considerable part of the luminescence comes from the defects accumulated by irradiation and that the intensities at these bands may reflect the amounts of the defects. Thus, similarly to the case of alumina [3], this in-situ luminescence measurement technique can be applied to monitor radiation-induced defects under irradiation; different irradiation time dependences which are observed for different specimens in Fig. 3 and for different temperatures in Fig. 4 can be analyzed to determine the production and reaction kinetics of the defects.

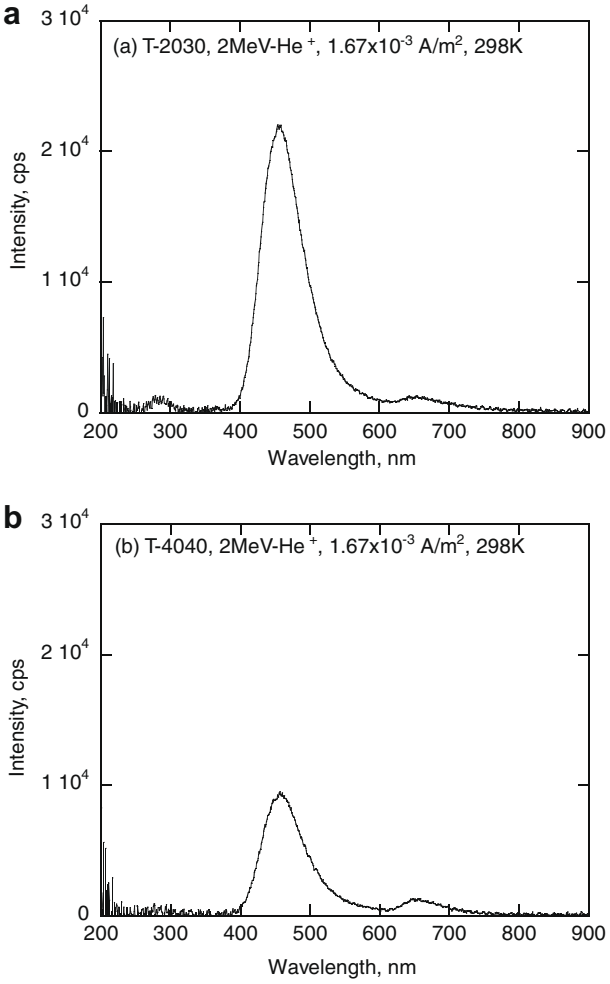

Fig. 1. Typical luminescence spectra of (a) T-2030 and (b) T-4040 under 2 MeV He^+ irradiation at 298 K. The specimen was annealed above 1073 K for 10 min.

Contrary to the luminescence at 460 nm and 650 nm, no apparent irradiation time dependence was observed for the luminescence at 280 nm, and almost constant luminescence intensity was observed after the start of irradiation. It is interesting to note that the 280 nm emission is constant. One can consider the possibility that this S1 to S0 transition/emission only occurs on production while the T1 to S0 can be re-excited during irradiation. It seems that the energy gap for activation of ODCs by excited electrons or electron-hole pairs from S_0 to S_1 leading to the singlet (280 nm) emission is considerably high, and that ODCs are mostly activated to T_1 leading to the triplet (460 nm) emission.

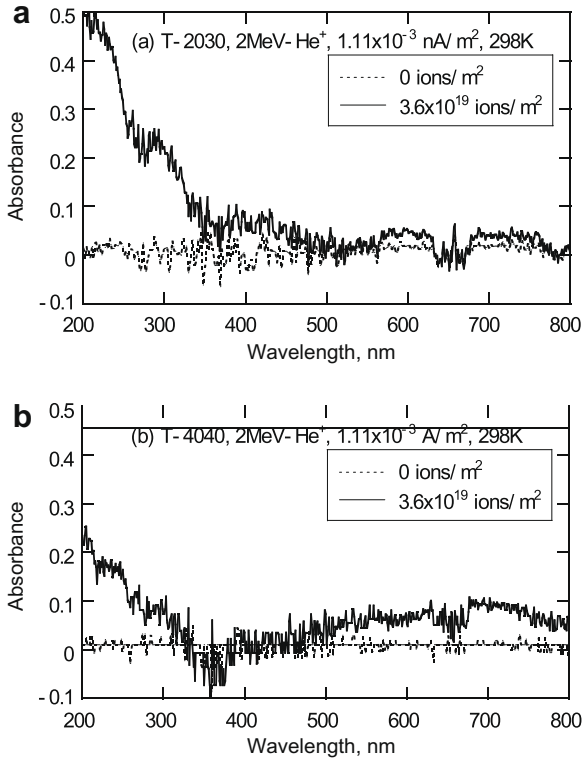

Fig. 2. Optical absorption spectra of (a) T-2030 and (b) T-4040 irradiated to 3.6×10^{19} ions m^{-2} by 2 MeV He^+.

3.2. Production and reaction mechanisms of radiation-induced defects

In the present study, it is reasonable to concentrate on the production and reaction mechanism of ODCs, of which the most intense luminescence at 460 nm is observed in the spectra. In the case of T-2030, it has been observed that the luminescence intensity at 460 nm increases after the start of irradiation and then decreases as shown in Fig. 3(a). Two possible reactions are considered for this decrease. One is the reaction of the ODCs with holes to produce the E' centers (≡Si•Si≡) [7], and the other the reaction of the ODCs to produce the higher order clusters, denoted by ODC_xs here. However, the former reaction is not enough to explain such a drastic decrease since a steady-state concentration is expected to be low for holes which mostly recombine with electrons. Thus the latter reactions of the ODCs are more likely to be responsible for the present observation. Taking into account these reactions, a typical reaction scheme of the ODCs is given by

$$SiO_2 \rightarrow SiO_2^* \rightarrow ODC + O \quad (0)$$

$$ODC + O \rightarrow SiO_2 \quad k_1 \quad (1)$$

$$O + A \rightarrow A' \quad k_2 \quad (2)$$

$$ODC + ODC \rightarrow ODC_x \quad k_3 \quad (3)$$

$$ODC + ODC_x \rightarrow ODC_x \quad k_4 \quad (4)$$

where k_i denotes the rate constant of reaction (i). Reaction (0) represents the production of an ODC, through an excited SiO_2 (SiO_2^*) by ion beam irradiation. Reaction (1) represents the recombination of the ODC with the O, and reaction (2) the competing reaction of the O in which the O is trapped by A to form A'. Reactions (3) and (4) represent the formation of cluster defects ODC_x. It is important to note that the reaction rate constants of k_3 and k_4 are treated as the same for a proper convergence in the following analysis. On the other hand, k_1 and k_2 are treated independently though the luminescence of the ODC may reflect the corresponding trapped counterpart (O interstitial) in the initial stage before ODC aggregation. The values of the rate constants are given in atomic fraction in the present study.

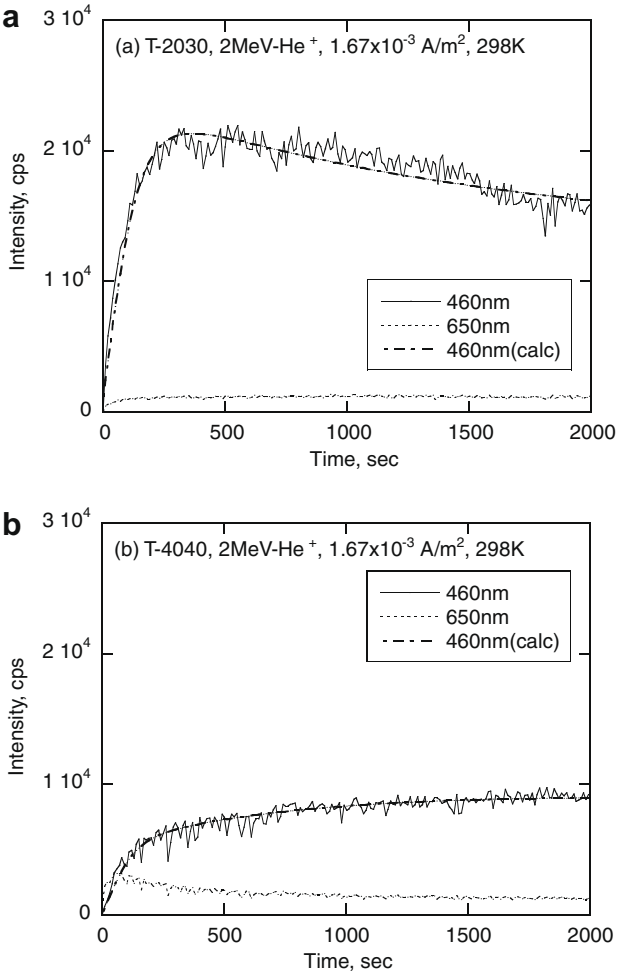

Fig. 3. Irradiation time dependence of the luminescence from (a) T-2030 and (b) T-4040 under 2 MeV He^+ irradiation. The specimen was annealed above 1073 K for 10 min.

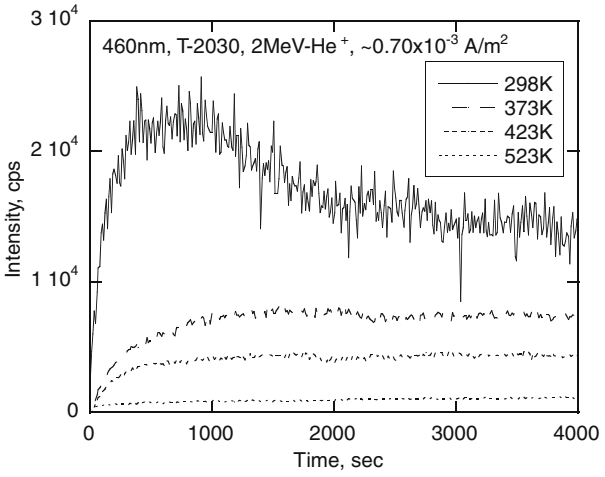

Fig. 4. Irradiation time dependence of the luminescence from T-2030 under 2 MeV He^+ irradiation at 298 K, 373 K, 423 K, and 523 K. The specimen was annealed above 1073 K for 10 min.

In the case of vitreous silica, there are known different defects and their reactions other than the above. Together with the diamagnetic centers of the ODCs, the paramagnetic centers of the E' centers, the peroxy radicals (PORs: ≡Si–O–O•Si≡), and the NBOHCs are known to be produced in this material [7]. It is also known that NBOHCs are formed with hydrogen atoms Hs in hydroxyl-containing silica (≡Si–OH) [9]. Some of those defects are considered to act as the O trapping centers; for example, the E' reacts with the O to form the NBOHC and the POR [10]. As reported for alkali halides [11], furthermore, there may be present the intrinsic O trapping centers as well as the extrinsic ones. For simplicity, the O trapping centers are represented by A inclusively, and reaction (2) is temporarily assumed to be of the first-order in the following analysis of the present data.

3.3. Determination of reaction rate constants

As mentioned above, the luminescence at 2.7 eV (460 nm) is attributed to the triplet (T_1 to S_0) [7]. Considering that the luminescence is caused from the ODCs activated by excited electrons or electron-hole pairs, the observed luminescence intensity I_{460} at 460 nm is proportional to the state density of [ODC(T_1)], as given by:

$$I_{460} = \varepsilon\phi[\mathrm{ODC}(T_1)] \tag{5}$$

where ε represents the luminescence detection efficiency including geometric factors and excitation probabilities and ϕ the ion beam current. The variation of the state density of [ODC(T_1)] with irradiation time can be calculated by solving the following equations:

$$\mathrm{d}[ODC]/\mathrm{d}t = g\phi - k_1[\mathrm{ODC}][O] - 2k_3[\mathrm{ODC}]^2 - k_4[\mathrm{ODC}][\mathrm{ODC}_x] \tag{6}$$

$$\mathrm{d}[O]/\mathrm{d}t = g\phi - k_1[\mathrm{ODC}][\mathrm{O}] - k_2[\mathrm{O}] \tag{7}$$

$$\mathrm{d}[\mathrm{ODC}_x]/\mathrm{d}t = k_3[\mathrm{ODC}]^2 \tag{8}$$

where g is the generation rate of ODCs and Os by reactions (0). One can estimate the g value from the conversion factor of 1 dpa (for oxygen) = 4.1×10^{20} ions/m^2 (2.0 MeV He$^+$). Considering the fractions of the surviving defects from cascade reactions, the g value is temporarily reduced by some factors in the present study; 0.1 for T-2030 and 0.05 for T-4040.

For the analysis of the observed results, Eqs. (6)–(8) are solved by the Runge–Kutta method to obtain the steady-state density of the ODC which is substituted into Eq. (5). As already mentioned above, the reaction rate constants of k_3 and k_4 are treated as the same for a proper convergence in the present analysis; k_3 for reactions (3) and (4) in both specimens. The measured luminescence intensity data were fitted to Eq. (5) combined with Eqs. (6)–(8) by the least-squares method, and the parameter values were obtained. As shown in Fig. 3, the agreements are satisfactorily good in all the cases.

As typical results of the present analysis, Fig. 5(a) and (b) show the variations of the defect densities with irradiation time in T-2030 and T-4040, respectively, which are simulated by using the obtained parameter values for the observed luminescence in Fig. 3(a) and (b). Different kinetics of the ODCs in T-2030 and T-4040 are shown in the figures. In the case of T-2030, the density of the ODCs increases rapidly and then decreases following the growth of the ODC$_x$s. In the case of T-4040, on the other hand, the density of the ODCs increases rather slowly with a slow growth of the ODC$_x$s. It is interesting to point out that the formation of the cluster defects ODC$_x$s starts above the dpa value of 10^{-3}. Very similar values are obtained in radiation studies where aggregation is important, including the results of such paramagnetic centers as the E' [12,13]. The dpa value of 10^{-3} corresponds to defects in every $10 \times 10 \times 10$ ion cell approximately, as an indication of the interaction length/range between the ODCs (or their counterpart, interstitials).

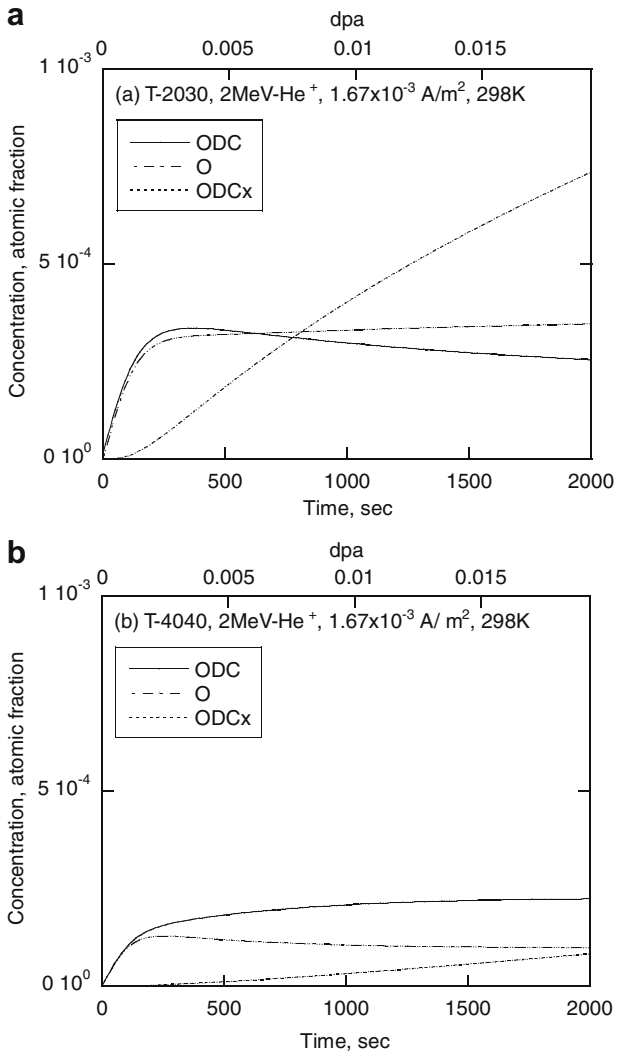

Fig. 5. Accumulation behavior of radiation-induced defects in (a) T-2030 and (b) T-4040 under 2 MeV He$^+$ irradiation. Curves represent the results of simulation for the observed luminescence in Fig. 2(a) and (b).

Fig. 6(a) and (b) show the Arrhenius plots of the rate constants of k_1, k_2 and k_3 (=k_4) for T-2030 and T-4040, respectively, which are obtained from the present analysis. As shown in Table 2, the Arrhenius equations of the rate constants are obtained by the least-squares fitting, and the activation energies are obtained for k_1, k_2 and k_3 (=k_4), in which some differences are found due to different OH contents in T-2030 (1 ppm OH) and T-4040 (800 ppm OH). In the case of T-2030, similar values of 0.44 and 0.39 eV are obtained for the activation energies of reactions (1) and (2), respectively, though the values are determined independently. This means that both reactions (1) and (2) are controlled in a similar way, possibly by the migration of the Os. In our recent study, the electron spin resonance measurement of irradiation defects and reactions in ion beam irradiated vitreous silica was performed in order to determine some rate constants [13]. In isothermal annealing experiments, sequential reactions of the E' centers with oxygen atoms to form the NBOHCs and PORs were observed to occur, and the activation energies were obtained to be about 0.4 eV for those reactions. The similarity of the activation energy values is thus considered to support the present interpretation of reactions (1) and (2).

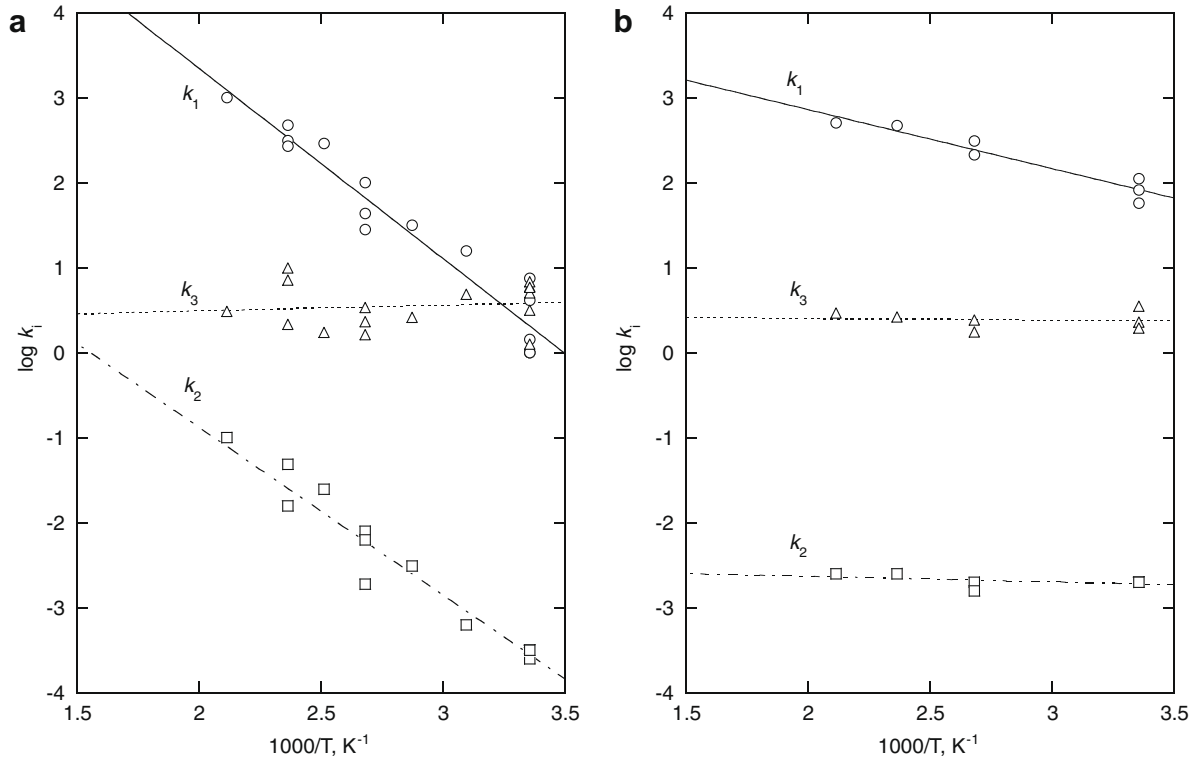

Fig. 6. Arrhenius plots of reaction rate constants, k_1, k_2 and k_3 for (a) T-2030 and (b) T-4040. Marks are experimental and curves represent the least-squares fits of the data to the Arrhenius equations.

Table 2
Reaction rate constants obtained from the analysis of in-situ luminescence measurement data.

Specimen	Rate constants	$k_i = A_i \exp[-E_i/kT]$		Note
		A_i	E_i (eV)	
T-2030	k_1	$10^{7.8\pm0.5}$	0.44 ± 0.03	
	k_2	$10^{3.1\pm0.3}$	0.39 ± 0.02	
	k_3	$10^{0.4\pm0.4}$	−0.01 ± 0.03	
	k_4	$(10^{0.4\pm0.4})$[a]	(−0.01 ± 0.03)[a]	
T-4040	k_1	$10^{4.2\pm0.3}$	0.14 ± 0.02	Effect of H
	k_2	$10^{-2.5\pm0.2}$	0.01 ± 0.01	Effect of H
	k_3	$10^{0.4\pm.3}$	0.00 ± 0.02	
	k_4	$(10^{0.4\pm0.3})$[a]	(0.00 ± 0.02)[a]	

[a] Assumed to be $k_3 = k_4$.

It is interesting to compare the present results with the literature ones. In the case of alkali halides, different types of oxygen interstitial traps, extrinsic and intrinsic, are known to be present and to affect the F-coloring and F-thermal-annealing curves [11]. Similarly to the case of alkali halides, there may be present different types of oxygen interstitial traps in vitreous silica. Under the present conditions of ion beam irradiation, however, an efficient defect production occurs and results in a relatively higher concentration of interstitials. The effects of various interstitial traps other than the E' centers and NBOHCs are thus considered to be negligible, similarly to the case of alumina [3] and alkali halides exposed to high dose [13].

In the case of T-4040, on the other hand, different values of 0.14 and 0.01 eV are obtained for reactions (1) and (2), respectively, in the analysis of the observations. For this difference due to different OH contents, it may be remembered that the hydrogen atoms, Hs, are formed from the OH (≡Si–OH) together with the NBOHCs as given by [4]:

$$\equiv Si - OH \rightarrow \equiv Si - O^{\cdot} + H \quad (9)$$

Considering a very rapid diffusion of the Hs [9,14], it is thus reasonable to assume that the Hs are affecting the reaction kinetics of the ODCs and Os in T-4040. Although further studies are needed, the Hs are considered to play an important role in the reaction kinetics of radiation-induced defects under irradiation.

As for the k_3 (=k_4), it is noticed that the activation energy of ~0 eV are considerably small compared with the others. This athermal behavior with zero activation energy may be compared with those reported in the early alkali halide work [15–17]. In that case, a similar athermal behavior was found for the production of anion vacancy aggregates (M or F_2 centers). Statistical production of the M centers by the F center production next to another stable F center was important in the initial stage, and a radiation enhanced term, also athermal, was reported in the later stage. Similarly to the alkali halide work, but by considering the formation of ion tracks, an explanation for the present case is given as follows. In the case of ion irradiation, there will be overlaps of ion tracks, which increase with the increasing dpa value. Then, defects once formed, including not only point defects of the ODCs but also cluster defects ODC_xs, may be involved in another ion track in which reactions (3) and (4) proceed. The activation energies of such reactions will be small as observed in the present study.

Finally it is important to note that no apparent temperature dependence of the luminescence detection efficiency is observed in the present measurement, as shown in Fig. 7. This means that no thermal quenching is observed. Although the efficiency values scatter by over one order of magnitude for T-2030 at the lowest temperature (298 K), no apparent dependence has been observed on the irradiation conditions such as the ion beam intensity. The efficiency values are considered to scatter possibly due to varying geometric factors in the repetitive measurements.

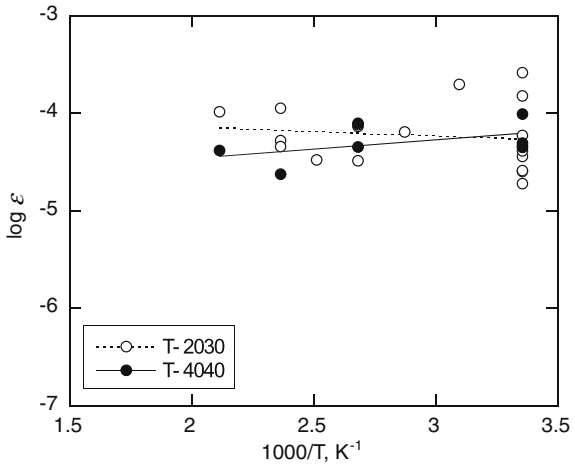

Fig. 7. Arrhenius plots of the luminescence detection efficiency of the ODCs. Marks are experimental.

4. Conclusions

The observed irradiation time dependence of the luminescence intensity under irradiation was confirmed to reflect the accumulation behavior of radiation-induced defects by its reproducibility with annealing. The results were successfully analyzed by considering a production and reaction mechanism of radiation-induced defects, which included the formation of cluster defects. By taking an estimated generation rate for point defects, the accumulation behavior of radiation-induced defects was obtained in the unit of atomic fraction. It was shown that the formation of the cluster defects ODC_x starts above the dpa value of 10^{-3}.

Acknowledgement

The authors wish to thank Mr. K. Yoshida, Kyoto University, for his kind experimental supports.

References

[1] H. Moriyama, S. Tanaka, K. Noda, J. Nucl. Mater. 258–263 (1998) 587.
[2] K. Moritani, I. Takagi, H. Moriyama, J. Nucl. Mater. 312 (2003) 97.
[3] K. Moritani, Y. Teraoka, I. Takagi, M. Akiyoshi, H. Moriyama, J. Nucl. Mater. 373 (2008) 157.
[4] L. Skuja, J. Non-Cryst. Solids 239 (1998) 16.
[5] W. Jiang, W.J. Weber, S. Thevuthasan, D.E. McCready, J. Nucl. Mater. 257 (1998) 295.
[6] N. Sekimuram, T. Iwai, Y. Arai, S. Yokomine, A. Naito, Y. Miwa, S. Hamada, J. Nucl. Mater. 283–287 (2000) 224.
[7] T. Ishizaki, Q. Xu, T. Yoshiie, S. Nagata, T. Troev, J. Nucl. Mater. 307–311 (2002) 961.
[8] M. Hattori, Y. Nishihara, Y. Ohki, M. Fujimaki, T. Souno, H. Nishikawa, T. Yamaguchi, E. Watanabe, M. Oikawa, T. Kamiya, K. Arakawa, Nucl. Instrum. and Meth. B 191 (2002) 362.
[9] A.R. Silin, L.N. Skuja, J. Mol. Struct. 61 (1980) 145.
[10] D.L. Griscom, M. Mizoguchi, J. Non-Cryst. Solids 239 (1998) 66.
[11] E.R. Hodgson, A. Delgado, J.L. Alvarez Rivas, Phys. Rev. B 18 (1978) 2911.
[12] K. Moritani, Y. Teraoka, I. Takagi, H. Moriyama, J. Nucl. Mater. 329–333 (2004) 988.
[13] J. Takemoto, K. Moritani, I. Takagi, M. Akiyoshi, H. Moriyama, J. Nucl. Mater. 374 (2008) 293.
[14] L.A. Shkrob, A.D. Trifunac, Phys. Rev. B 54 (1996) 15073.
[15] E.R. Hodgson, A. Delgado, J.L. Alvarez Rivas, J. Phys. C: Solid State Phys. 12 (1979) 1239.
[16] E.R. Hodgson, A. Delgado, J.L. Alvarez Rivas, J. Phys. C: Solid State Phys. 12 (1979) 4393.
[17] E.R. Hodgson, A. Delgado, J.L. Alvarez Rivas, J. Phys. C: Solid State Phys. 14 (1981) 337.